Anti-CD30 diabody-drug conjugates with potent antitumor activity

Kristine M. Kim, Charlotte F. McDonagh, Lori Westendorf, Lindsay L. Brown, Django Sussman, Tiffany Feist, Robert Lyon, Stephen C. Alley, Nicole M. Okeley, Xinqun Zhang, Melissa C. Thompson, Ivan Stone, Hans-Peter Gerber, and Paul J. Carter

Seattle Genetics, Inc., Bothell, Washington

Abstract

Anti-CD30 diabodies were engineered with two cysteine mutations for site-specific drug conjugation in each chain of these homodimeric antibody fragments. Diabodies were conjugated with ~4 equivalents of the anti-tubulin drugs, monomethyl auristatin E or F, via a protease-cleavable dipeptide linker, to create the conjugates, diabody-vcE4 and diabody-vcF4, respectively. Diabody conjugation had only minor (<3-fold) effects on antigen binding. Diabody-vcF4 was potently cytotoxic against the antigen-positive cell lines, Karpas-299 (34 pmol/L IC_{50}) and L540cy (22 pmol/L IC_{50}), and was 8- and 21-fold more active than diabody-vcE4 against these cell lines, respectively. Clearance of diabody-vcF4 (99-134 mL/d/kg) was 5-fold slower than for the nonconjugated diabody in naive severe combined immunodeficient mice. Diabody-vcF4 had potent and dose-dependent antitumor activity against established Karpas-299 xenografts and gave durable complete responses at well-tolerated doses. Biodistribution experiments with diabody-[^{3}H]-vcF4 (0.72-7.2 mg/kg) in tumor-bearing mice showed a dose-dependent *increase* in total auristatin accumulation in tumors (≤520 nmol/L) and *decrease* in relative auristatin accumulation (≤8.1 %ID/g), with peak localization at 4 to 24 h after dosing. Diabody-vcF4 had ~4-fold lower cytotoxic activity than the corresponding IgG1-vcF4 conjugate *in vitro*. A similar potency difference was observed *in vivo* despite 25- to 34-fold faster clearance of diabody-vcF4 than IgG1-vcF4. This may reflect that dose-escalated diabody-vcF4 can surpass IgG1-vcF4 in auristatin delivery to tumors, albeit with higher auristatin exposure to some organs including kidney and liver. Diabody-drug conjugates can have potent antitumor activity at well-tolerated doses and warrant further optimization for cancer therapy. [Mol Cancer Ther 2008;7(8):2486–97]

Introduction

Twelve antibody-based drugs have been approved for anticancer therapy including 9 by the U.S. Food and Drug Administration (1, 2). These antibody therapeutics provide significant benefit to some patients but are seldom curative. Antibody conjugation to cytotoxic drugs is one of the most promising ways to enhance the antitumor activity of antibodies and to reduce the systemic toxicity of the conjugated drugs (3–5). Indeed, one antibody-drug conjugate (ADC) is approved for human therapy, gemtuzumab ozogamicin (Mylotarg), for the treatment of acute myeloid leukemia (6). Ten ADCs are in clinical trials as of May 2008, including Mylotarg (5). This progress has encouraged further improvements to enhance the clinical potential of ADCs (3–5), including engineering of the IgG delivery vehicle (7), and the use of alternative antibody formats as described here.

Antibody localization to tumors in cancer patients is commonly inefficient, 0.0003 to 0.08 %ID/g tumor (8) even with antibodies with exquisite selectivity for tumor over normal tissue (9). Drug conjugation seems unlikely to improve tumor uptake of IgG. Indeed, preclinical studies revealed that conjugation of the maytansinoid drug, DM1, to the humanized antibody, huC242, had *no* significant effect on antibody biodistribution in tumor-bearing mice (10). Thus, catabolism distant from tumor site is the presumed ultimate fate of the majority of an administered ADC dose and a potential source of toxicity.

Usage of antibody fragments such as diabodies (11) to construct drug conjugates offers a potential way to circumvent the catabolic fate of IgG-drug conjugates. This reflects that diabodies, unlike IgG, are eliminated rapidly and primarily by renal filtration (12, 13). If antibody fragment drug conjugates are excreted with drug still attached, this will lessen the exposure of nontumor sites to free drug and potentially reduce the toxicity observed with IgG-drug conjugates. Diabodies (50-55 kDa) are smaller than IgG (~150 kDa) and this can facilitate more rapid tumor penetration and accumulation (14). Nevertheless, tumor accumulation of diabodies is ≥2-fold lower than for corresponding IgG (3, 15). This reflects that the more rapid tumor penetration of diabodies is more than offset by faster clearance than IgG due to smaller size and lack of binding to the salvage receptor, FcRn.

The ADC, SGN-35 (16), comprises a chimeric anti-CD30 IgG1 antibody (17) conjugated to the potent cytotoxic drug, monomethyl auristatin E, via a protease-cleavable

Received 4/23/08; revised 6/4/08; accepted 6/6/08.

The costs of publication of this article were defrayed in part by the payment of page charges. This article must therefore be hereby marked *advertisement* in accordance with 18 U.S.C. Section 1734 solely to indicate this fact.

Note: K.M. Kim and C.F. McDonagh contributed equally to this work.

Current address for P.J. Carter: VLST, Inc., 307 Westlake Avenue North, Suite 300, Seattle, WA 98100.

Current address for C.F. McDonagh: Merrimack Pharmaceuticals, One Kendall Square, Cambridge, MA 02139.

Requests for reprints: Kristine M. Kim, Seattle Genetics, Inc., 21823 30th Drive Southeast, Bothell, WA 98021. Phone: 425-527-4644; Fax: 425-527-4609. E-mail: kkim@seagen.com

doi:10.1158/1535-7163.MCT-08-0388

valine-citrulline linker (18). SGN-35 has a mean loading of ~4 drugs/antibody and induced complete regressions of established tumor xenografts at doses well below those maximally tolerated (16). SGN-35 is well tolerated and has elicited multiple objective responses in a phase I clinical trial for $CD30^+$ hematologic malignancies (19).

Here, anti-CD30 diabodies were engineered with cysteine residues for site-specific conjugation to monomethyl auristatin E (18) or F (20). Anti-CD30 diabody-drug conjugates were compared with the corresponding anti-CD30 IgG1-drug conjugates with respect to CD30 binding and *in vitro* cytotoxic activity against $CD30^+$ and $CD30^-$ cell lines. The most potent anti-CD30 diabody-drug conjugate, diabody-vcF4, was compared with the corresponding IgG1-drug conjugate, IgG1-vcF4, in pharmacokinetic, efficacy, biodistribution, and safety studies in mice.

Materials and Methods

Cell Lines

The anaplastic large cell lymphoma line, Karpas-299 ($CD30^+$), and the non-Hodgkin's lymphoma cell line, WSU-NHL ($CD30^-$), were obtained from the Deutsche Sammlung von Mikroorganism und Zellkulturen. L540cy ($CD30^+$), a derivative of the Hodgkin's lymphoma cell line L540 adapted to xenograft growth, was developed by Dr. Harald Stein (Institüt für Pathologie, University Veinikum Benjamin Franklin). Cell lines were grown in RPMI 1640 (Life Technologies) supplemented with either 10% (v/v; Karpas-299 and WSU-NHL) or 20% (v/v; L540cy) fetal bovine serum.

Diabody Design

Genes encoding the variable domains of the anti-CD30 monoclonal antibody, AC10 (17), were reformatted as diabodies (11) in the mammalian expression vector pcDNA4mycHis (Invitrogen). Anti-CD30 diabodies were created in both possible topologies, V_H-G_3SG_4 linker-V_L (diabody-HL) and V_L-G_3SG_4 linker-V_H (diabody-LH). The diabodies included a COOH-terminal hexahistidine tag for purification by immobilized metal affinity chromatography. Subsequent constructs were based on diabody-HL as this format, unlike diabody-LH, had the expected size-exclusion high-performance liquid chromatography (HPLC) properties (see Results).

A three-dimensional model of the AC10 Fv fragment was generated to facilitate the design of diabody Ser→Cys mutants for site-specific drug conjugation. The AC10 model was created by threading the AC10 variable domain sequences onto the structure of a murine single-chain Fv fragment (PDB code: 1qok; ref. 21) using the Phyre-Server protein structure prediction application (22) from the Equinox Pay-Per-Use Web site.[1] Model accuracy was judged by the *e*-value (0.0e00) and estimated threading precision (100%) plus appropriate placement of the antigen-binding complementarity determining regions and putative loop residues as confirmed by visual inspection.

Guided by molecular modeling, selected serine residues (see Results) in AC10 diabody-HL were mutated to cysteine using pairs of complementary oligonucleotide primers by QuikChange Mutagenesis (Stratagene). Three different anti-CD30 diabody-HL-Cys variants were created, each containing two cysteine replacement mutants per polypeptide chain, there by providing four cysteine sites per diabody for drug conjugation. Specifically, diabody-HL-Cys1 contains the V_H S84C mutation and the Cys linker (G_3SCG_3), diabody-HL-Cys2 contains the V_L S14C mutation and the Cys linker, and diabody-HL-Cys3 contains the two variable domain Cys mutations in conjunction with the original linker (G_3SG_4). A control diabody was generated from the anti-p97/melanotransferrin monoclonal antibody, L49 (23). Specifically, L49 diabody-HL-Cys1 was generated by gene synthesis (Blue Heron Biotechnology) in the V_H-linker-V_L (HL) topology, with the V_H S84C mutation and the Cys linker (G_3SCG_3) for drug conjugation.

Diabody and IgG1 Production

Diabodies were transiently expressed in HEK 293F cells (Invitrogen) following transfection of corresponding pcDNA4 expression constructs with 293fectin (Invitrogen) or PEI (Polysciences) as recommended by their vendors. Cells were cultured for 8 days in F17 Medium (Invitrogen) before diabody purification from the conditioned medium. For stable production of AC10 diabody-HL-Cys1 and L49 diabody-HL-Cys1, corresponding genes were subcloned downstream of the CHEF EF-1α promoter in the mammalian expression vector, pDEF38 (24). Linearized pDEF38 expression constructs were electroporated into CHO-DG44 cells (25). Stably transfected CHO pools and CHO clones expressing diabodies were selected in hypoxanthine- and thymidine-deficient Ex-cell 325 medium (SAFC Biosciences). AC10 diabody-HL-Cys1 CHO clones and the L49 diabody-HL-Cys1 CHO pool were cultured in Ex-cell 325 medium in shake flasks or 5 to 10 L Wave bioreactors (Wave Biotech) for 14 days.

Diabodies were purified by immobilized metal affinity chromatography using a HisTrap column (GE Healthcare; see Supplementary Material).[2] Purified diabodies were dialyzed against PBS, 50 mmol/L imidazole, 1 mmol/L EDTA, and 5% (v/v) glycerol (pH 8.0) and then analyzed by SDS-PAGE and TSK-Gel G3000SW HPLC size-exclusion chromatography (Tosoh Bioscience). The anti-CD30 IgG1 (cAC10) stably expressed in CHO-DG44 cells and control IgG1 (anti-CD19, cHD37) transiently expressed in HEK 293F cells were purified by protein A chromatography as described for cAC10 IgG1 (7).

Diabody and IgG1 Conjugation to Auristatins

Anti-CD30 (AC10) and control (L49) diabodies were conjugated via their engineered cysteine residues to maleimidocaproyl-valine-citrulline-*p*-aminobenzyloxycarbonyl-monomethylauristatin E (mc-vcMMAE; ref. 18) or

[1] http://www.equinoxppu.com

[2] Supplementary materials for this article are available at Molecular Cancer Therapeutics Online (http://mct.aacrjournals.org/).

maleimidocaproyl-valine-citrulline-*p*-aminobenzyloxycarbonyl-monomethylauristatin F (mc-vcMMAF; ref. 20). Diabodies were incubated with 5 mmol/L Tris(2-carboxyethyl)-phosphine (TCEP) at 37°C for 1.5 h to reduce the intrachain disulfide bond apparently formed between the two engineered cysteine residues (see Results). Excess TCEP was removed by dialysis, and mc-vcMMAE or mc-vcMMAF was then added in slight excess to produce an average loading of 3.7 drugs per diabody. The identities of the resultant conjugates were confirmed by liquid chromatography-mass spectrometry using a PLRP-S reverse-phase column (Polymer Labs) coupled to a QTOF-API high-resolution mass spectrometer (Waters). Diabody-drug conjugates were immediately frozen and stored at −80°C until use. The anti-CD30 and control chimeric IgG1 were partially reduced using 2.5 equivalents of TCEP for 90 min at 37°C and then conjugated to mc-vcMMAE or mc-vcMMAF as described previously (7, 20, 26).

Custom synthesized [^{3}H]-mc-vcMMAF (Moravek Biochemicals) was used to prepare radiolabeled anti-CD30 diabody-HL-Cys1-vcF4 and anti-CD30 IgG1-vcF4 conjugates for biodistribution studies. [^{3}H]-mc-vcMMAF was labeled with a single ^{3}H atom in the *meta*-position of the COOH-terminal phenylalanine at 21 Ci/mmol. Reduction of the diabody and IgG1 for radioconjugation were carried out as described above. Reduction reactions were placed on ice and then treated with a mixture of [^{3}H]-mc-vcMMAF (1.0 mCi/mL in ethanol) and unlabeled mc-vcMMAF in a proportion determined to generate drug conjugates with a specific activity of ~60 to 70 μCi/mg. Conjugation was allowed to proceed for 45 and 15 min on ice for the IgG1 and diabody, respectively. Any remaining drug linker was quenched with *N*-acetylcysteine for 15 min. The diabody conjugate was used without further purification, whereas the IgG was purified by three rounds of centrifugal filtration with PBS (Amicon Ultra, 30 kDa MWCO) or until <0.1% of the radioactivity eluted in the flow through. Drug loadings were estimated using PLRP chromatography (7, 26) and specific activities of the conjugates were determined by UV/visible spectroscopy and liquid scintillation counting.

Cell Binding by Diabody and IgG1-Drug Conjugates

Competition binding of the anti-CD30 diabody-drug and IgG1-drug conjugates was undertaken using CD30$^+$ Karpas-299 cells and either europium-labeled cAC10 IgG1 as described (7) or cAC10 labeled with Alexa Fluor 488 (Molecular Probes/Invitrogen) at 2.0 μg/mL. Alexa Fluor samples were analyzed using a LSRII flow cytometer (BD Bioscience) and mean fluorescence intensity data were converted using Winlist 5.0 (Verity Software House). Data were baseline corrected using Prism v4.01 (GraphPad Software) and reported as the percent of maximum fluorescence as calculated by the sample fluorescence divided by the fluorescence of cells stained with cAC10-europium or cAC10-Alexa Fluor 488 alone.

Cytotoxicity of Diabody and IgG1-Drug Conjugates

Growth inhibition of CD30$^+$ Karpas-299 or L540cy cells and CD30$^-$ WSU-NHL cells treated with diabody and IgG1-drug conjugates was determined by incubating conjugates with cells for 92 h followed by incubation with 50μmol/L resazurin for 4 h at 37°C as described (7). Dye reduction was measured using a Fusion HT microplate reader. Data were analyzed by a nonlinear least squares fit to a four-variable logistic equation using Prism v4.01.

Pharmacokinetics of Diabody, IgG1, and Their Drug Conjugates

Pharmacokinetics of the anti-CD30 diabody and the diabody-vcF4 conjugate were evaluated in female severe combined immunodeficient (SCID) mice (Harlan). Groups of mice (n = 3) were administered with 2.16 or 7.2 mg/kg of the anti-CD30 diabody or diabody-vcF4 conjugate by tail vein injection. Blood samples were collected from each mouse via the saphenous vein at 0.083, 0.25, 0.5, 1, 2, 4, 8, 16, 24, 48, 72, 120, and 168 h after injection. Serum samples were isolated and stored at −80°C before estimation of the serum concentration of total diabody by Luminex assay. All animal experiments were conducted under Institutional Animal Care and Use Committee guidelines and approval.

Diabody and diabody-drug conjugate were captured with Luminex beads labeled with an anti-idiotype antibody to cAC10 in Luminex buffer [20 mmol/L Tris-HCl (pH 8.0), 150 mmol/L NaCl, 0.05% (w/v) Tween 20, 0.1% (w/v) bovine serum albumin, 0.05% (w/v) sodium azide (pH 7.4)] for 1 h at room temperature in the dark. Plates were washed twice with Luminex buffer and incubated for 1 h at room temperature in the dark with anti-pentaHis-Alexa Fluor 532 conjugate (Qiagen). Plates were washed twice and read on a Luminex 200 (Luminex). The diabody and diabody-drug conjugate pharmacokinetic data were subjected to both noncompartmental and compartmental analysis using WinNonlin version 4.0.1 (Pharsight).

Pharmacokinetics of the anti-CD30 IgG1-vcF4 conjugate were determined as described previously for the corresponding anti-CD30 IgG1-vcE4 conjugate (27), with minor modifications. Groups (n = 3) of female SCID mice (Harlan) were administered with 10 mg/kg IgG1-vcF4 by tail vein injection. Blood samples were collected from each mouse via the saphenous vein at 0.042, 0.25, 1, 2, 4, 7, 14, 21, 28, and 35 days after injection. Serum samples were isolated and stored at −80°C before analysis by antigen-binding ELISA for total immunoglobulin. IgG1-vcF4 pharmacokinetic data were subjected to noncompartmental analysis with WinNonlin version 4.0.1.

Tumor Xenograft Efficacy Experiments with Diabody and IgG1-Drug Conjugates

Karpas-299 cells (5×10^6) were implanted into the right flank of C.B-17 SCID mice (Harlan) to establish a s.c. disease model of anaplastic large cell lymphoma (18, 27, 28). Tumor-bearing mice were randomly divided into groups (n = 8-9) when the mean tumor volume was 100 mm^3. Test groups were treated with a single i.v. dose of 0.72, 2.16, or 7.2 mg/kg anti-CD30 diabody-vcF4 or 0.66, 2.0, or 6.0 mg/kg anti-CD30 IgG1-vcF4. Control groups received a single i.v. dose of 7.2 mg/kg anti-CD30 diabody, 7.2 mg/kg negative control diabody-vcF4, 6.0 mg/kg anti-CD30 IgG1, or 6.0 mg/kg negative control IgG1-vcF4. An additional

control group was left untreated. Tumor volume was calculated using the formula: $(A \times B^2) / 2$, where A and B are the largest and second largest perpendicular tumor dimensions, respectively. Animals were euthanized when tumor volumes reached ~1,000 mm^3.

Biodistribution of Diabody and IgG1-Drug Conjugates

Groups of SCID mice ($n = 3$) bearing s.c. Karpas-299 tumors of ~100 mm^3 prepared as for the efficacy experiments were treated with a single i.v. dose of 0.72, 2.16, or 7.2 mg/kg anti-CD30 diabody-[^{3}H]-vcF4 or 2.0 mg/kg anti-CD30 IgG1-[^{3}H]-vcF4. Serum, tissue (spleen, liver, kidney, intestine, bladder, stomach, lung, bone, and tumor), and intestine contents (ingesta) samples were collected at 1, 4, 8, 16, 24, and 48 h after dosing. Tissues were homogenized on ice after the addition of 1.2 mL methanol. Total radioactivity (antibody bound auristatin plus free auristatin) of the homogenate was determined by removing a 200 μL aliquot, mixing with 4 mL Ecoscint A (National Diagnostics), and liquid scintillation counting. Soluble radioactivity (free auristatin) was determined by centrifuging the remaining homogenate at 16,000 × g for 5 min. A supernatant aliquot (200 μL) was removed and mixed with 4 mL Ecoscint A and scintillations were counted. The %ID/g values were calculated by dividing the μCi [^{3}H] found in a tissue sample by the μCi [^{3}H] injected into the animal and then dividing by the mass of the tissue sample in grams. Total auristatin (antibody bound auristatin plus free auristatin) and free auristatin concentrations were calculated using the specific activity of the radioactive drug. Lung and bone samples could not be processed reliably using the methods described above and were therefore omitted from subsequent analysis.

Maximum Tolerated Dose of Diabody and IgG1-Drug Conjugates

Groups of female SCID mice ($n = 3$) were injected with the anti-CD30 diabody-vcF4 or IgG1-vcF4 conjugates via the tail vein to determine the multiple-dose maximum tolerated dose. The dosing regimen for diabody-vcF4 was 2.16, 3.24, 4.32, or 6.48 mg/kg every 4 days for four doses. IgG1-vcF4 was dosed at 1.0, 3.0, 6.0, and 9.0 mg/kg every 4 days for four doses. An untreated control group ($n = 3$) was also included. Mice were monitored daily for 14 days, and weight and clinical observations were recorded. Mice that developed significant signs of distress were euthanized.

Statistical Analysis of Antitumor Efficacy Data

Tumor growth delay was calculated using the formula: tumor growth delay = $[(T - C) / C] \times 100\%$, where T and C are the median tumor quadrupling times in days for treated and untreated control groups, respectively. Tumor quadrupling times were determined by nonlinear regression analysis for exponential growth for each individual animal based on the tumor volume at the beginning of treatment (day 1 for this analysis). Animals that did not reach the endpoint were assigned an endpoint value equal to the last day of the study. Student's t test (two-tailed) was applied using Prism 5 (GraphPad Software) to analyze the differences in median tumor quadrupling time between groups of mice. Differences were deemed significant where $P \leq 0.05$.

Results

Diabody Design for Site-Specific Drug Conjugation

Diabodies (11) of the anti-CD30 monoclonal antibody, AC10 (17), were designed in which the antigen-binding variable domains were connected by means of an 8-residue linker, G_3SG_4. Both possible topologies were generated, V_H-linker-V_L (diabody-HL) and V_L-linker-V_H (diabody-LH), to explore whether one orientation offers advantages over the other (Fig. 1A).

Our preferred method for conjugating cytotoxic drugs to antibodies is via solvent accessible cysteine residues distant from the antigen-binding complementarity determining regions (18). Drug conjugation at these sites is anticipated to *not* affect antigen binding as shown for the anti-CD30 IgG1, cAC10 (7). Suitable solvent-accessible cysteine residues for drug conjugation are lacking in diabodies and were therefore introduced by site-directed mutagenesis.

An AC10 Fv homology model was built by threading the corresponding amino acid sequences onto the crystallographic structure of a murine single-chain Fv fragment (PDB code: 1qok, ref. 21). Three different residues were selected for cysteine replacement mutagenesis. Specifically the serine residues, V_H S84 and V_L S14 (Kabat numbering; ref. 29), were selected based on their solvent accessibility and location in framework region loops that are distant from the complementarity determining regions (Fig. 1B). A third site was selected in the G_3SG_4 linker connecting the V_H and V_L domains. Three different diabody Cys variants were designed, each containing two Cys→Ser replacements per polypeptide chain, thus giving rise to four cysteine sites per diabody for drug conjugation. Specifically, diabody Cys1 contains the V_H S84C mutation and the Cys linker (G_3SCG_3), diabody Cys2 contains the V_L S14C mutation and the Cys linker, and diabody Cys3 contains the two variable domain Cys mutations in conjunction with the original linker (G_3SG_4).

Production of Diabody and IgG1 Drug Conjugates

The parent anti-CD30 diabodies, diabody-HL and diabody-LH, were transiently expressed in HEK 293F cells and purified by immobilized metal affinity chromatography using the COOH-terminal hexahistidine tag. Diabody-HL eluted as a single major peak by size-exclusion chromatography consistent with the anticipated 52.8-kDa dimer, whereas diabody-LH had a more complex chromatogram, consistent with the presence of multiple species (Fig. 1C). Diabody-HL was therefore selected as the backbone for installing the cysteine mutations for site-specific drug conjugation described above and for all subsequent work.

Diabody-HL Cys1, diabody-HL Cys2, and diabody-HL Cys3 variants were transiently expressed and purified similar to the parent diabodies and analyzed by SDS-PAGE (Fig. 1D). Diabody-HL-Cys1 and diabody-HL-Cys2 gave rise to single major band close to that expected (26.4 kDa) with similar yields to the parent diabody-HL (1-4 mg/L). In contrast, diabody-HL-Cys3 was recovered in lower yield (150 μg/L) and apparently formed at least one interchain disulfide bond, as judged by electrophoresis under nonreducing conditions (Fig. 1D). Diabody-HL-Cys1 had slightly

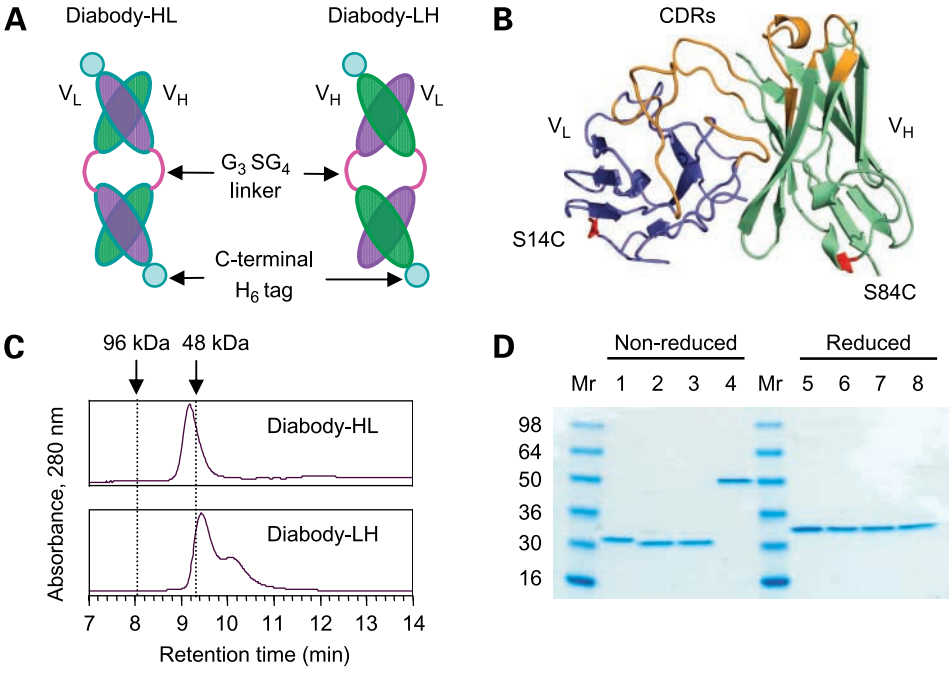

Figure 1. Diabody design and biochemical characterization. **A,** alternative diabody formats comprising V_H (*olive green*) and V_L (*mauve*) domains connected in both possible orientations by a G_3SG_4 octapeptide linker (*magenta*): diabody-HL (V_H-linker-V_L) and diabody-LH (V_L-linker-V_H). Also shown is a COOH-terminal hexahistidine tag (*blue*). **B,** homology structural model of AC10 anti-CD30 Fv fragment highlighting V_H (*olive green*) and V_L (*mauve*) domains, the complementarity determining region loops (*orange*) as defined structurally (44), and mutations V_H S84C and V_L S14C (*red*) for site-specific drug attachment. **C,** size-exclusion HPLC chromatographs of the parent diabodies, diabody-HL and diabody-LH. **D,** SDS-PAGE analysis of diabody-HL variants done under nonreducing or reducing conditions: *lanes 1* and *5,* parent; *lanes 2* and *6,* Cys1; *lanes 3* and *7,* Cys2; *lanes 4* and *8,* Cys3.

more favorable physiochemical characteristics than diabody-HL-Cys2 (e.g., greater solubility and lower tendency to aggregate) and was chosen as the lead diabody for drug conjugation. Diabody-HL-Cys1 was stably expressed in a CHO-DG44 cell line at titers of ~24 mg/L. This diabody was purified from 5 to 10 L cultures by immobilized metal affinity chromatography with >95% purity as assessed by SDS-PAGE (data not shown).

For diabody-HL-Cys1, the mass of 26,408 Da observed by time-of-flight mass spectrometry closely matches the expected mass of 26,408.3 Da if all six cysteines, including the two engineered cysteines, participate in intrachain disulfide bonds (Supplementary Fig. S1).[2] Consistent with this notion, no free thiols were detected for diabody-HL-Cys1. Moreover, treatment of diabody-HL-Cys1 with excess TCEP produced a small shift in retention time by reverse-phase HPLC associated with a mass of 26,410 Da (Supplementary Fig. S1).[2] This 2-Da mass increase is consistent with selective reduction of a single disulfide bond per diabody chain. Diabody-HL-Cys1 was conjugated to the auristatin drug-linkers, mc-vcMMAE (18) and mc-vcMMAF (20), to generate drug conjugates hereafter called ''diabody-vcE4'' and ''diabody-vcF4,'' respectively. These diabody-drug conjugates contained ~3.7 drugs/diabody (Table 1), close to the anticipated 4 drugs/diabody. The observed mass of the component chains of diabody-vcF4 was 29,072 Da (Supplementary Fig. S1),[2] in good agreement with the expected mass of 29,071.5. The chimeric anti-CD30 IgG1, cAC10 (17), was conjugated with mc-vcMMAE and mc-vcMMAF to generate previously described ADCs (7, 20, 26) with a mean loading of ~4 drugs/antibody and are called hereafter as ''IgG1-vcE4'' and ''IgG1-vcF4,'' respectively (Table 1).

In vitro Characterization of Diabody, IgG1, and Their Drug Conjugates

The alternative antibody formats, diabody or IgG1, and drug conjugation had only minor (<3-fold) effects on binding to the cognate antigen, CD30, as shown by competition binding experiments using europium or Alexa Fluor 488–labeled anti-CD30-IgG1 (cAC10) with $CD30^+$ cells (Table 1). Drug conjugation with vcMMAE endowed the diabody with potent *in vitro* cytotoxic activity against $CD30^+$ cell lines, Karpas-299 and L540cy, as judged by subnanomolar IC_{50} values in cytotoxicity assays (Table 1). Cytotoxic potency of the diabody-drug conjugate was increased 8- and 21-fold by selection of mc-vcMMAF over mc-vcMMAE for Karpas-299 and L540cy cell lines, respectively. Nevertheless, diabody-vcF4 was 4.1- and 2.4-fold *less* potent than IgG1-vcF4 against the $CD30^+$ cell lines, Karpas-299 and L540cy, respectively. All anti-CD30 conjugates (Table 1) had low (IC_{50} > 10 nmol/L) or no cytotoxic activity against the $CD30^-$ cell line, WSU-NHL, whereas a positive control conjugate, anti-CD19 IgG1-vcF4, had potent activity (IC_{50} = 9 pmol/L) against this cell line. Diabody-vcF4 and IgG1-vcF4 are the most potent drug conjugates in the two different antibody formats and were selected for *in vivo* activity comparisons.

Pharmacokinetics of Diabody, IgG1, and Their Drug Conjugates

SCID mice were dosed with the anti-CD30 diabody or diabody-vcF4 conjugate to investigate their pharmacokinetic properties including the effect of drug conjugation (Fig. 2). Doses of 2.16 and 7.2 mg/kg were chosen to match efficacy experiments (Fig. 3). Clearance of diabody-vcF4 was 5-fold *slower* than for the nonconjugated diabody at both 2.16 and 7.2 mg/kg doses (Fig. 2A and *B*; Table 2). The

area under the curve (AUC) was 5-fold greater for diabody-vcF4 than the nonconjugated diabody, as anticipated because clearance is calculated by dividing the dose by the AUC. The β half-life ($t_{1/2}\beta$) is the half-life of the second phase in a two (or more) compartment pharmacokinetic model. For diabody-vcF4 and diabody, $t_{1/2}\beta$ estimates were comparable: ~4-6 h (Table 2). Increasing the diabody-vcF4 dose 3-fold from 2.16 to 7.2 mg/kg increased the AUC by 4.5-fold, with only minor differences in other pharmacokinetic variables (Table 2).

The pharmacokinetics of the anti-CD30 diabody and diabody-vcF4 conjugate were compared with those of the corresponding anti-CD30 IgG1, cAC10 (27), and its drug conjugate, IgG1-vcF4 (Fig. 2). Clearance of diabody-vcF4 was 25- to 34-fold faster and $t_{1/2}\beta$ 59- to 85-fold shorter than for IgG1-vcF4 depending on the dose. In contrast, only minor differences were observed between the pharmacokinetic properties of the anti-CD30 IgG1 (27) and its corresponding drug conjugate, IgG1-vcF4 (Fig. 2C; Table 2).

In vivo Efficacy of Diabody and IgG1-Drug Conjugates

Single dose efficacies of anti-CD30 diabody-vcF4 and IgG1-vcF4 were compared in an established (~100 mm^3) s.c. tumor xenograft model of anaplastic large cell lymphoma (Karpas-299) in SCID mice (Fig. 3). Diabody-vcF4 conjugate showed potent and dose-dependent antitumor activity with 0 of 9, 6 of 9, and 7 of 9 complete responses, defined here as no detectable tumor for at least 5 successive measurements, at 0.72, 2.16, and 7.2 mg/kg doses, respectively (Fig. 3A). The median delay in tumor quadrupling time at 0.72, 2.16, and 7.2 mg/kg doses of diabody-vcF4 versus the untreated control was 35% ($P = 0.0011$), 207% ($P < 0.0001$), and 261% ($P < 0.0001$). In contrast, the nonconjugated anti-CD30 diabody and the nonbinding control diabody-vcF4 conjugate did *not* show antitumor activity in this model. Diabody-vcF4 has lower antitumor potency than IgG1-vcF4 when matched for relative amounts of auristatin (shown in parentheses) administered: 0.72 mg/kg diabody-vcF4 (1×) versus 2.0 mg/kg IgG1-vcF4 (1×; $P < 0.0001$). The magnitude of this potency difference is ~3-fold as suggested by the following efficacy comparisons: 0.72 mg/kg diabody-vcF4 (1×) versus 0.66 mg/kg IgG1-vcF4 (0.3×; $P = 0.21$), 2.16 mg/kg diabody-vcF4 (3×) versus 2.0 mg/kg IgG1-vcF4 (1×; $P = 0.13$), and 7.2 mg/kg diabody-vcF4 (10×) versus 6.0 mg/kg IgG1-vcF4 (3×; $P = 0.06$).

Multiple-Dose Maximum Tolerated Dose of Diabody and IgG1-Drug Conjugates

Maximum tolerated dose was defined as the highest dose that did *not* induce ≥20% weight loss or severe signs of distress. Determination of a single-dose maximum tolerated dose for diabody-vcF4 in mice was not feasible as this conjugate was well tolerated and susceptible to aggregation when concentrated above ~2 mg/mL. The multiple-dose maximum tolerated dose of diabody-vcF4 and IgG1-vcF4 were determined as ≥6.8 and ≥9.0 mg/kg, respectively, when given every 4 days times 4. The single-dose maximum tolerated dose for the anti-CD30 IgG1-vcF4 in BALB/c mice is 50 mg/kg (20).

Biodistribution of Diabody and IgG1-Drug Conjugates

Tumor targeting of the anti-CD30 diabody-[^{3}H]-vcF4 and IgG1-[^{3}H]-vcF4 conjugates was investigated in tumor-bearing mice using variables selected to match the efficacy experiments. Groups of mice ($n = 3$) with established (~100 mm^3) s.c. Karpas-299 tumors were injected via their tail with a single dose of diabody-[^{3}H]-vcF4 at 0.72, 2.16, or 7.2 mg/kg or alternatively IgG1-[^{3}H]-vcF4 at 2.0 mg/kg. Total auristatin and free auristatin retention in tumor, blood, other tissues, and ingesta were determined for up to 48 h after dosing. Time courses for both total auristatin and free auristatin in different samples were evaluated as %ID/g (Fig. 4). The data were also analyzed in concentration units (nmol/L) to better understand the relationships between diabody-[^{3}H]-vcF4 dose and auristatin delivery (Fig. 4).

Diabody-[^{3}H]-vcF4 showed a dose-dependent *increase* in total auristatin accumulation in tumors and reaching peak concentrations of 100, 220, and 520 nmol/L for the 0.72, 2.16, and 7.2 mg/kg doses, respectively, at 4 to 24 h after dosing. In contrast, there was a dose-dependent *decrease* in

Table 1. *In vitro* characterization of anti-CD30 diabody and IgG1 and their auristatin drug conjugates

Anti-CD30 antibody or drug conjugate	Drugs per diabody or IgG1*	Competition binding Karpas-299 (IC_{50}, nmol/L)†	Cytotoxicity‡	
			Karpas-299 (IC_{50}, pmol/L)	L540cy (IC_{50}, pmol/L)
Diabody	0	2.3 ± 0.3	No effect	No effect
Diabody-vcE4	3.7	6.6 ± 1.2	269 ± 19	470 ± 110
Diabody-vcF4	3.7	3.8 ± 0.2	33.6 ± 2.5	22.3 ± 5.4
IgG1	0	5.1 ± 0.2	No effect	No effect
IgG1-vcE4	4	3.0 ± 0.6	28.6 ± 2.6	51.0 ± 9.4
IgG1-vcF4	4.5	6.3 ± 0.3	8.1 ± 0.9	9.3 ± 2.2

NOTE: Mean ± SE are from three or more independent experiments.

*The diabody loading with auristatins was determined by reverse-phase HPLC (7, 26), whereas the loading of the IgG1 was determined by both reverse-phase and hydrophobic interaction chromatography methods (27).

†Competition binding experiments were undertaken using europium or Alexa Fluor 488–labeled anti-CD30 IgG1 (cAC10) and $CD30^+$ cells (Karpas-299), which gave indistinguishable results.

‡The cytotoxicity assays (96 h) used either $CD30^+$ cells (Karpas-299 and L540cy, as shown) or $CD30^-$ cells (WSU-NHL; see Results).

relative total auristatin accumulation in tumors for the diabody conjugate with a peak of ~8.1, 6.3, and 4.3 %ID/g for the 0.72, 2.16, and 7.2 mg/kg doses, respectively, at 4 to 24 h after dosing. The IgG1 conjugate localized more efficiently to tumors than the diabody conjugate and continue to accrue throughout the experiment reaching ~26 %ID/g by 48 h. Diabody-[^{3}H]-vcF4 (0.72 mg/kg) matched for auristatin dose with IgG1-[^{3}H]-vcF4 (2.0 mg/kg) resulted in ~3-fold lower concentrations of total auristatin accumulating in the tumor. However, increasing the dose of diabody-drug conjugate by 3-fold (2.16 mg/kg) or 10-fold (7.2 mg/kg) matched or surpassed the total auristatin delivery to the tumor from the IgG1 conjugate (2.0 mg/kg)

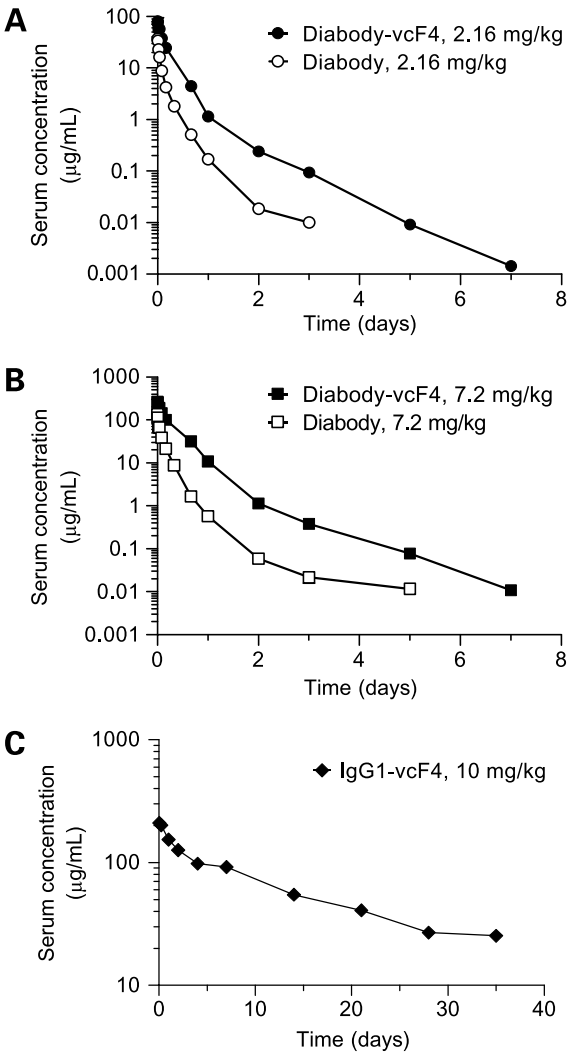

Figure 2. Pharmacokinetics of anti-CD30 diabody, diabody-vcF4, and IgG1 in SCID mice. Mice (n = 3 per group) were injected via their tail vein with diabody or diabody-vcF4 at 2.16 mg/kg (**A**) or 7.2 mg/kg (**B**) and serum samples were collected and analyzed by Luminex fluid array sandwich immunoassay to determine the total diabody concentration. **C,** mice were treated with the anti-CD30 IgG1-vcF4 conjugate and serum samples were collected and analyzed by antigen-binding ELISA to determine the total IgG concentration.

up to 24 h, respectively. Between 24 and 48 h, a minor reduction and a modest additional tumor accumulation of total auristatin was observed for the diabody and IgG1 conjugates, respectively. Free auristatin accumulation in tumors from the diabody and IgG1 conjugates showed very similar trends to total auristatin accrual, albeit at slightly reduced levels (up to ~2-fold lower).

Diabody-[^{3}H]-vcF4 cleared much more rapidly from serum than did IgG1-[^{3}H]-vcF4, consistent with the pharmacokinetic studies (Fig. 2; Table 2). Virtually no free auristatin was found in the serum. In contrast, for some other samples, such as liver and ingesta, the free auristatin levels approached the levels of total auristatin. In some cases, the total auristatin was much higher than the free auristatin (e.g., IgG1 conjugate in kidney and bladder). The highest concentrations of free auristatin detected (high nanomolar to low micromolar range) were in the ingesta and liver samples. These data are consistent with hepatobiliary excretion being a major route of elimination of auristatin for both diabody and IgG1 conjugates. The high concentrations of free auristatin observed in the intestine samples likely reflect, at least in part, carryover from the ingesta. Additionally, the diabody conjugate, but not the IgG1 conjugate, gave similar levels of total and free auristatin in the kidney and bladder. These data support the notion of renal clearance being an additional route of elimination of auristatin from diabody conjugates. However, excretion studies are required to confirm the routes, magnitudes, and kinetics of auristatin elimination as well as to determine if auristatin is still attached to diabody putatively eliminated via the kidney. The methodology used cannot distinguish between auristatin and derived metabolites.

Tumor-to-tissue exposure ratios ($AUC_{0\text{-}48\ h}$ tumor/$AUC_{0\text{-}48\ h}$ tissue) were calculated for both total auristatin and free auristatin (Table 3). For the diabody conjugate, these exposure ratios were similar for free and total auristatin, with the exception of the serum, where the exposure ratio was 19- to 26-fold higher for free auristatin. Diabody and IgG1 conjugates are prodrugs with no antitumor activity until the auristatin is released. Thus, free auristatin rather than total auristatin exposure ratios represent the more relevant measure of targeted versus nontargeted activity. All free auristatin comparisons show greater exposure ratios for the IgG1 conjugate than for the diabody conjugate.

Discussion

Diabodies have previously been successfully engineered for site-specific conjugation at two sites per diabody using a COOH-terminal cysteine residue or a linker cysteine (30, 31). Here, an anti-CD30 diabody was engineered for efficient site-specific drug conjugation at four sites per diabody with minimal affect on antigen binding. This was achieved by novel serine-to-cysteine replacements (V_H S84C or V_L S14C) in solvent accessible framework region loops distant from the antigen-binding complementarity determining regions in conjunction with a cysteine-containing

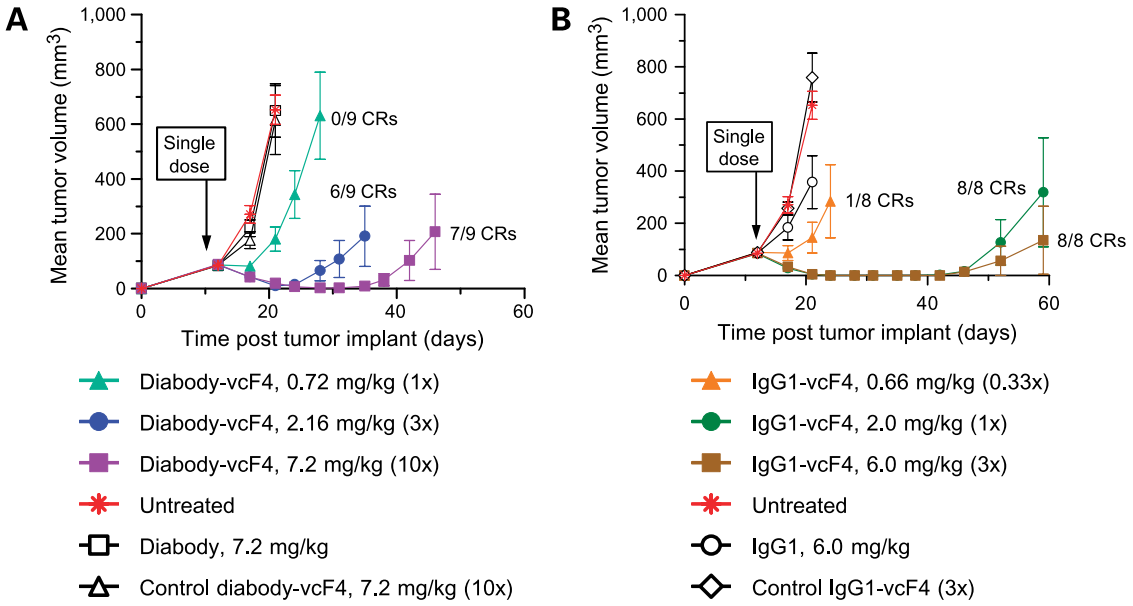

Figure 3. Single dose efficacy of anti-CD30 diabody-vcF4 and IgG1-vcF4 conjugates in SCID mice (n = 8 or 9 per group) bearing established s.c. Karpas-299 tumor xenografts. Mean tumor volumes were plotted for each group until one or more animals died or was euthanized (see Materials and Methods). Mean ± SE are representative of independent experiments. Relative auristatin doses are shown in parentheses. Complete response is defined here as no detectable tumor for at least five successive measurements. Student's t test (see Materials and Methods) was used to analyze the differences in median tumor quadrupling time between groups (see Results).

octapeptide linker, G_3SCG_3. In addition to the anti-CD30 diabody (Table 1), this site-specific conjugation strategy was successfully applied to a negative control diabody and is potentially broadly applicable to other diabodies.

Diabodies with engineered cysteine residues have been expressed in *Escherichia coli* (32), *Pichia pastoris* (33), NS0 (30, 31), HEK 293 and CHO (this work). Diabodies with engineered cysteines sometimes form interchain disulfide bonds depending on the location of the cysteines and the production host. Engineered interchain disulfide bonds impair diabody expression in some cases (32), but not others (31), as further exemplified here. The pairs of engineered cysteine residues in the well-expressed diabody variant, Cys1 (Fig. 1), efficiently formed an intrachain disulfide bond as judged by mass spectrometry before and after reduction with TCEP. Our molecular modeling together with some available diabody structures (34, 35) are consistent with disulfide bond formation between the two engineered cysteines. Indeed, the structures place V_H S84C in the vicinity of the linker cysteine. Reduction of this putative engineered disulfide bond permitted efficient and site-specific drug conjugation (Table 1). Olafsen et al. described a diabody with a single engineered cysteine that formed an interchain disulfide bond (31). This disulfide bond was reduced to permit site-specific conjugation to a radionuclide chelator for *in vivo* imaging.

The anti-CD30 diabody and its auristatin drug conjugates showed similar competition binding properties to each other as well as to the corresponding IgG1 and its drug conjugates (Table 1). In contrast, the diabody conjugates showed 2- to 9-fold lower cytotoxic activity than the corresponding IgG1 conjugates depending on the auristatin

Table 2. Pharmacokinetics of anti-CD30 diabody, anti-CD30 IgG1, and their corresponding auristatin F drug conjugates in SCID mice

Anti-CD30	Dose (mg/kg)	$t_{1/2}\beta$ (days)	AUC (d μg/mL)	Clearance (mL/d/kg)
Diabody	2.16	0.18 ± 0.01	3.24 ± 0.09	668 ± 18
Diabody	7.2	0.16 ± 0.01	13.5 ± 0.3	532 ± 12
Diabody-vcF4	2.16	0.16 ± 0.01	16.3 ± 1.3	134 ± 10
Diabody-vcF4	7.2	0.23 ± 0.01	73.0 ± 3.4	98.9 ± 4.5
IgG1	10	16.7 ± 0.1	2,640 ± 40	3.8 ± 0.1
IgG1-vcF4	10	13.6 ± 0.4	2,600 ± 100	3.9 ± 0.2

NOTE: Pharmacokinetic variables (mean ± SE, n = 3 mice per group) were estimated by noncompartmental analysis, except for $t_{1/2}\beta$ for diabody and diabody-vcF4 that were calculated from a compartmental analysis. This approach was taken as $t_{1/2}\beta$ for the diabody and diabody-vcF4 could not be reliably estimated by noncompartmental analysis due to the observed triphasic disposition. The pharmacokinetic data for the anti-CD30 IgG1, cAC10, were reported previously by Hamblett et al. (27).

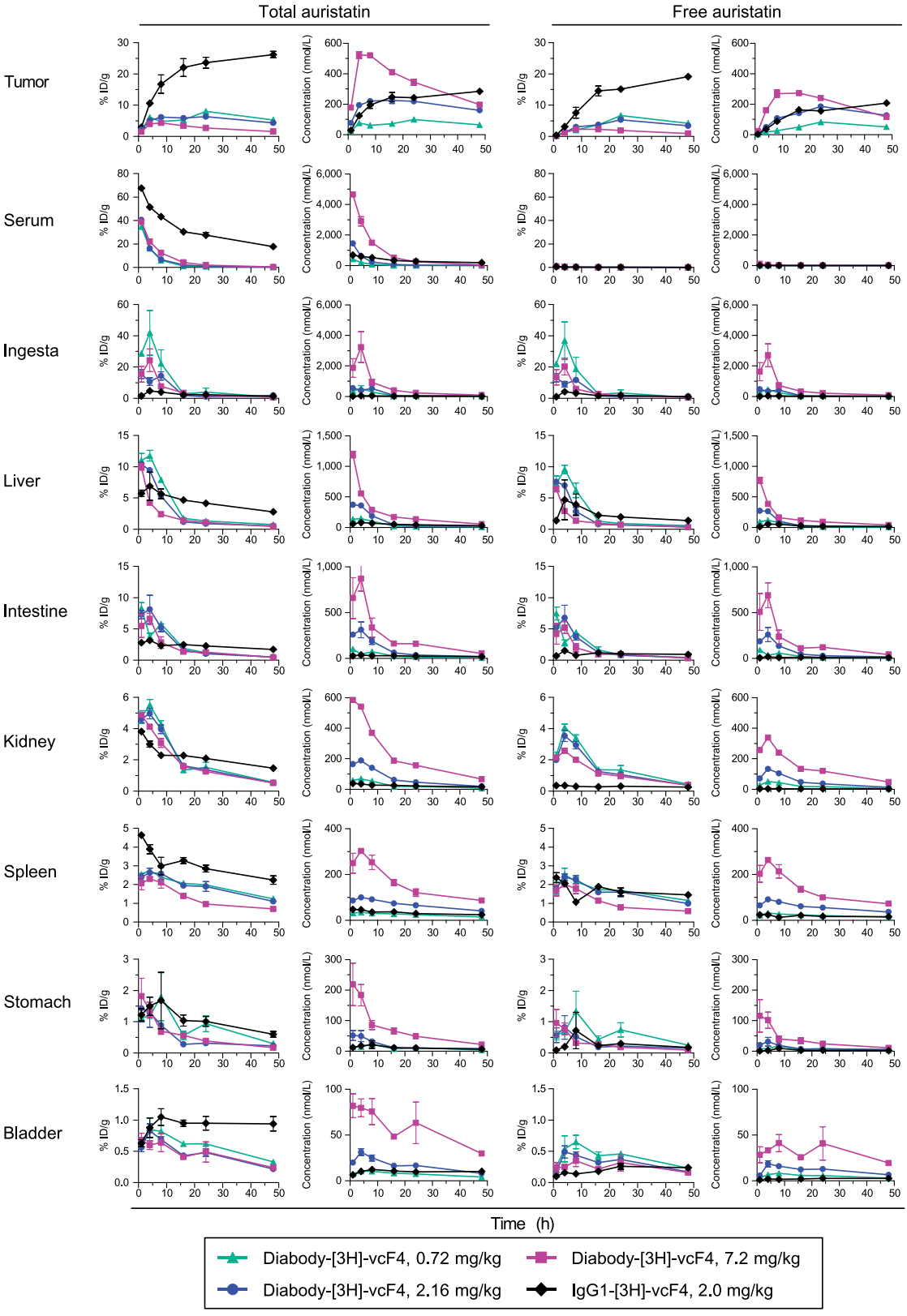

Figure 4. Biodistribution of anti-CD30 diabody-[^{3}H]-vcF4 and IgG1-[^{3}H]-vcF4 conjugates in SCID mice bearing established (100 mm^3) s.c. Karpas-299 tumor xenografts. Mean ± SE for groups of three mice.

drug and the cell line. Drug loading differences between diabody and IgG1 conjugates were minor (Table 1) and unlikely to account for potency differences. The difference in properties of diabody and IgG1 conjugates presumably reflects difference in spatial orientation of the two antigen binding sites between these alternative antibody formats. Other potential, and as yet unexplored, mechanisms for the lower potency of the diabody conjugates include differences in rates of internalization, net accumulation of drug, intracellular trafficking, or drug release from the conjugates.

Diabody-vcF4 was the most potent anti-CD30 diabody-drug conjugate and was selected for *in vivo* evaluation alongside the nonconjugated diabody, the corresponding IgG1 and its drug conjugate, IgG1-vcF4. Drug conjugation to the diabody reduced the clearance in naive SCID mice by 5-fold. The observed mass of 29,072 Da for the individual component chains of diabody-vcF4 is only 2,662 Da greater than for the TCEP-reduced and nonconjugated diabody, consistent with the addition of two equivalents of the drug-linker (Supplementary Fig. S1).[2] Additionally, only a small increase in apparent size of diabody-vcF4 over nonconjugated diabody was shown by the relatively low resolution method of size-exclusion chromatography HPLC (~47 versus ~38 kDa, respectively; Supplementary Fig. S2).[2] Thus, drug conjugation to diabody results in only small increases in molecular weight and apparent size that do not appear to offer a plausible explanation for the slower pharmacokinetic clearance of diabody-vcF4 compared with the nonconjugated diabody. Another possibility is that auristatin drug conjugation may affect the routes and rate of diabody elimination (see below). In contrast to clearance differences, $t_{1/2}\beta$ estimates from compartmental analysis were similar for diabody and diabody conjugates (4-6 h) and fall within the range of previously reported for diabodies (3, 15).

Diabody-vcF4 had potent and dose-dependent antitumor activity against established Karpas-299 xenografts and gave rise to durable complete responses at well-tolerated doses (Fig. 3). Indeed, the *in vivo* potency of diabody-vcF4 was only ~3- to 4-fold lower than for IgG1-vcF4 (see Results), comparable with the difference in *in vitro* cytotoxicity for these conjugates with the Karpas-299 cell line. This potent antitumor activity of diabody-vcF4 is striking given that the clearance of this conjugate is 25- to 34-fold faster than for IgG1-vcF4 depending on the dose (Table 2). However, the efficacy data correlate with both total and free auristatin concentrations in the tumor in a matched biodistribution experiment. Specifically, increasing the diabody-drug conjugate by 3- or 10-fold over IgG1-vcF4 based on auristatin matched or surpassed the auristatin delivery to the tumor from the IgG1 conjugate, respectively, at least over the first 24 h after dosing (Fig. 4).

Peak tumor accumulation of [^{3}H]-auristatin for the diabody-drug conjugate (4.3-8.1%ID/g, depending on dose) is in the range of 3 to 14 %ID/g reported previously for biodistribution studies with diabodies labeled with radioiodine (31, 36–38) and radiometals (30, 39) targeting a variety of different tumor antigens and tumors. The time required for the diabody-drug conjugate to reach its peak tumor accumulation (4-24 h) is slightly longer than previously reported for radiolabeled diabodies (1-6 h; refs. 30, 31, 36–39).

The biodistribution data (Fig. 4) are consistent with hepatobiliary and renal elimination being major and minor routes, respectively, for auristatin excretion from diabody-drug conjugates. In contrast, several previous biodistribution studies with radiolabeled diabodies are consistent

Table 3. Biodistribution of anti-CD30 diabody-[^{3}H]-vcF4 and IgG1-[^{3}H]-vcF4

	Tumor $AUC_{0\text{-}48\ h}$/tissue $AUC_{0\text{-}48\ h}$			
	0.72 mg/kg diabody-vcF4	2.16 mg/kg diabody-vcF4	7.2 mg/kg diabody-vcF4	2.0 mg/kg IgG1-vcF4
Total auristatin				
Serum	1.7	1.3	0.5	0.7
Ingesta	0.7	1.3	0.6	8.6
Liver	1.9	2.3	1.7	4.9
Intestine	2.8	2.4	1.6	9.4
Kidney	3	2.9	1.7	10.1
Spleen	3.2	3	2.3	7.3
Stomach	7.3	11.7	5.4	20.1
Bladder	10.4	11.9	6.3	22.6
Free auristatin				
Serum	31.8	32.5	12.8	77.2
Ingesta	0.6	1.1	0.4	6.9
Liver	1.8	2.3	1.5	5.7
Intestine	2.6	2.1	1.2	13.2
Kidney	2.7	2.8	1.5	45.9
Spleen	2.6	2.4	1.6	8.5
Stomach	7	13	6.2	43.4
Bladder	10.4	11.7	6.4	63.7

NOTE: $AUC_{0\text{-}48\ h}$ ratios were calculated from the time-concentration biodistribution data (Fig. 4).

with renal elimination being the major excretion mechanism for diabodies (30, 31, 36–39). Hepatobiliary elimination of auristatins has been shown previously for trastuzumab-vcMMAE (40). The notion that diabody conjugation to auristatins promotes hepatobiliary elimination warrants investigation through excretion studies.

For diabody-[^{3}H]-vcF4 kidney accumulation of radioactivity is lower than reported previously for radiolabeled diabody conjugates (30, 31, 36–39). However, the kidney levels of free auristatin are within ~2-fold of the total auristatin present, consistent with some catabolism of the diabody-drug conjugate in the kidney. For radiolabeled antibody fragments, rapid glomerular filtration is apparently followed by readsorption in the proximal tubules via luminal endocytosis, leading to high levels of radioactivity in the kidney (41). Several strategies have been developed to reduce renal levels of radioactivity from radiolabeled antibody fragments (42). Some of these strategies have been applied successfully to diabodies, including blockade of renal readsorption using D-lysine (39), and are potentially applicable to diabody-drug conjugates. Incorporating a protease-cleavable linker between a Cys-diabody and a radionuclide chelator also attenuated kidney levels of radioactivity (30). Diabody-vcF4 includes a valine-citrulline dipeptide linker between the diabody and the drug. Linker proteolysis releases auristatin F, a negatively charged molecule with limited cell permeability (20). Thus, extracellular linker cleavage seems unlikely to result in cellular accumulation of auristatin F, whereas this seems more likely to occur if the diabody-drug conjugate is internalized and the drug released following linker cleavage. If necessary, auristatin E could be used for diabody conjugation, albeit with reduced activity (Table 1). Auristatin E, in contrast to auristatin F, is uncharged and apparently freely cell membrane permeable (20).

IgG-drug conjugates are a relatively mature modality optimized over several decades for potent antitumor activity and acceptable safety. In contrast, this current work is, to our knowledge, the first description of a diabody-drug conjugate, albeit not yet optimized. *In vitro* screening of large panels of IgG-drug conjugates can be used to identify highly potent ADCs (5). Moreover, the therapeutic index of IgG drug conjugates can be improved by optimizing the number of drugs per antibody (27). Screening large panels of diabody-drug conjugates and optimizing the drug loading offer potential ways to improve the efficacy and therapeutic index of diabody-drug conjugates. In addition to drug conjugation, other strategies are showing promise for ''payloading'' diabodies for cancer therapy. For example, conjugation of anti-HER2/*neu* diabodies to the α-emitting radioisotope, ^{211}At, have recently been shown to delay significantly the growth of established human breast cancer xenografts (43).

Disclosure of Potential Conflicts of Interest

K.M. Kim, C.F. McDonagh, L. Westendorf, L.L. Brown, R. Lyon, S.C. Alley, N.M. Okeley, X. Zhang, I. Stone, P.J. Carter: past or present employees of Seattle Genetics, Inc.; ownership interest in Seattle Genetics, Inc. D. Sussman, T. Feist, M.C. Thompson, H-P. Gerber: past or present employees of Seattle Genetics, Inc.

Acknowledgments

We thank Francisco Zapata and Drs. Carmel Lynch and Bhaskar Rege for assistance with pharmacokinetic experiments and data analysis and Christine Hansen for purification of the negative control diabody.

References

1. Liu XY, Pop LM, Vitetta ES. Engineering therapeutic monoclonal antibodies. Immunol Rev 2008;222:9–27.

2. Reichert JM, Valge-Archer VE. Development trends for monoclonal antibody cancer therapeutics. Nat Rev Drug Discov 2007;6:349–56.

3. Wu AM, Senter PD. Arming antibodies: prospects and challenges for immunoconjugates. Nat Biotechnol 2005;23:1137–46.

4. Lambert JM. Drug-conjugated monoclonal antibodies for the treatment of cancer. Curr Opin Pharmacol 2005;5:543–9.

5. Carter PJ, Senter PD. Antibody-drug conjugates for cancer therapy. Cancer J 2008;14:154–69.

6. Bross PF, Beitz J, Chen G, et al. Approval summary: gemtuzumab ozogamicin in relapsed acute myeloid leukemia. Clin Cancer Res 2001;7:1490–6.

7. McDonagh CF, Turcott E, Westendorf L, et al. Engineered antibody-drug conjugates with defined sites and stoichiometries of drug attachment. Prot Eng Des Sel 2006;19:299–307.

8. Sedalacek H-H, Seemann G, Hoffmann D, et al. Antibodies as Carriers of Cytotoxicity, Vol. 43. Munich (Germany): Karger; 1992.

9. Scott AM, Lee FT, Tebbutt N, et al. A phase I clinical trial with monoclonal antibody ch806 targeting transitional state and mutant epidermal growth factor receptors. Proc Natl Acad Sci U S A 2007;104:4071–6.

10. Xie H, Audette C, Hoffee M, Lambert JM, Blättler WA. Pharmacokinetics and biodistribution of the antitumor immunoconjugate, cantuzumab mertansine (huC242–1), and its two components in mice. J Pharmacol Exp Ther 2004;308:1073–82.

11. Holliger P, Prospero T, Winter G. ''Diabodies'': small bivalent and bispecific antibody fragments. Proc Natl Acad Sci U S A 1993;90:6444–8.

12. Wu AM, Yazaki PJ. Designer genes: recombinant antibody fragments for biological imaging. Q J Nucl Med 2000;44:268–83.

13. Colcher D, Pavlinkova G, Beresford G, Booth BJ, Choudhury A, Batra SK. Pharmacokinetics and biodistribution of genetically-engineered antibodies. Q J Nucl Med 1998;42:225–41.

14. Graff CP, Wittrup KD. Theoretical analysis of antibody targeting of tumor spheroids: importance of dosage for penetration, and affinity for retention. Cancer Res 2003;63:1288–96.

15. Holliger P, Hudson PJ. Engineered antibody fragments and the rise of single domains. Nat Biotechnol 2005;23:1126–36.

16. Hamblett KJ, Barton J, Cerveny CG, et al. SGN-35, an anti-CD30 antibody-drug conjugate, exhibits potent antitumor activity for the treatment of CD30+ malignancies. Blood 2005;106:Abstract 610.

17. Wahl AF, Klussman K, Thompson JD, et al. The anti-CD30 monoclonal antibody SGN-30 promotes growth arrest and DNA fragmentation in vitro and affects antitumor activity in models of Hodgkin's disease. Cancer Res 2002;62:3736–42.

18. Doronina SO, Toki BE, Torgov MY, et al. Development of potent monoclonal antibody auristatin conjugates for cancer therapy. Nat Biotechnol 2003;21:778–84.

19. Younes A, Forero-Torres A, Bartlett NL, et al. Objective responses in a phase I dose-escalation study of SGN-35, a novel antibody-drug conjugate (ADC) targeting CD30, in patients with relapsed or refractory Hodgkin lymphoma. J Clin Oncol 2008;Abstract #8526.

20. Doronina SO, Mendelsohn BA, Bovee TD, et al. Enhanced activity of monomethylauristatin F through monoclonal antibody delivery: effects of linker technology on efficacy and toxicity. Bioconjug Chem 2006;17:114–24.

21. Boehm MK, Corper AL, Wan T, et al. Crystal structure of the anti-(carcinoembryonic antigen) single-chain Fv antibody MFE-23 and a model for antigen binding based on intermolecular contacts. Biochem J 2000;346:519–28.

22. Bennett-Lovsey RM, Herbert AD, Sternberg MJ, Kelley LA. Exploring the extremes of sequence/structure space with ensemble fold recognition in the program Phyre. Proteins 2008;70:611–25.

23. Siemers NO, Kerr DE, Yarnold S, et al. Construction, expression, and activities of L49-sFv-b-lactamase, a single-chain antibody fusion protein for anticancer prodrug activation. Bioconjug Chem 1997;8:510 – 9.

24. Running Deer J, Allison DS. High-level expression of proteins in mammalian cells using transcription regulatory sequences from the Chinese hamster EF-1alpha gene. Biotechnol Prog 2004;20:880 – 9.

25. Urlaub G, Mitchell PJ, Kas E, et al. Effect of gamma rays at the dihydrofolate reductase locus: deletions and inversions. Somat Cell Mol Genet 1986;12:555 – 66.

26. Sun MM, Beam KS, Cerveny CG, et al. Reduction-alkylation strategies for the modification of specific monoclonal antibody disulfides. Bioconjug Chem 2005;16:1282 – 90.

27. Hamblett KJ, Senter PD, Chace DF, et al. Effects of drug loading on the antitumor activity of a monoclonal antibody drug conjugate. Clin Cancer Res 2004;10:7063 – 70.

28. Francisco JA, Cerveny CG, Meyer DL, et al. cAC10-vcMMAE, an anti-CD30-monomethyl auristatin E conjugate with potent and selective antitumor activity. Blood 2003;102:1458 – 65.

29. Kabat EA, Wu TT, Perry HM, Gottesman KS, Foeller C, editors. Sequences of Proteins of Immunological Interest, 5th ed. Bethesda (MD): NIH; 1991.

30. Li L, Olafsen T, Anderson AL, Wu A, Raubitschek AA, Shively JE. Reduction of kidney uptake in radiometal labeled peptide linkers conjugated to recombinant antibody fragments. Site-specific conjugation of DOTA-peptides to a Cys-diabody. Bioconjug Chem 2002;13:985 – 95.

31. Olafsen T, Cheung CW, Yazaki PJ, et al. Covalent disulfide-linked anti-CEA diabody allows site-specific conjugation and radiolabeling for tumor targeting applications. Protein Eng Des Sel 2004;17:21 – 7.

32. Zhu Z, Presta LG, Zapata G, Carter P. Remodeling domain interfaces to enhance heterodimer formation. Protein Sci 1997;6:781 – 8.

33. FitzGerald K, Holliger P, Winter G. Improved tumour targeting by disulphide stabilized diabodies expressed in *Pichia pastoris*. Protein Eng 1997;10:1221 – 5.

34. Pei XY, Holliger P, Murzin AG, Williams RL. The 2.0-Å resolution crystal structure of a trimeric antibody fragment with noncognate VH-VL domain pairs shows a rearrangement of VH CDR3. Proc Natl Acad Sci U S A 1997;94:9637 – 42.

35. Perisic O, Webb PA, Holliger P, Winter G, Williams RL. Crystal structure of a diabody, a bivalent antibody fragment. Structure 1994;2: 1217 – 26.

36. Adams GP, Schier R, McCall AM, et al. Prolonged in vivo tumour retention of a human diabody targeting the extracellular domain of human HER2/neu. Br J Cancer 1998;77:1405 – 12.

37. Khawli LA, Biela B, Hu P, Epstein AL. Comparison of recombinant derivatives of chimeric TNT-3 antibody for the radioimaging of solid tumors. Hybrid Hybridom 2003;22:1 – 9.

38. Wu AM, Chen W, Raubitschek A, et al. Tumor localization of anti-CEA single-chain Fvs: improved targeting by non-covalent dimers. Immunotechnol 1996;2:21 – 36.

39. Yazaki PJ, Wu AM, Tsai SW, et al. Tumor targeting of radiometal labeled anti-CEA recombinant T84.66 diabody and t84.66 minibody: comparison to radioiodinated fragments. Bioconjug Chem 2001;12:220 – 8.

40. Pastuskovas CV, Maruoka EM, Shen BQ, et al. Tissue distribution, metabolism, and excretion of the antibody-drug conjugate Herceptin-monomethyl auristatin E in rats. Proc Am Assoc Cancer Res 2005;46: Abstract #5063.

41. Arano Y, Fujioka Y, Akizawa H, et al. Chemical design of radiolabeled antibody fragments for low renal radioactivity levels. Cancer Res 1999;59: 128 – 34.

42. Arano Y. Strategies to reduce renal radioactivity levels of antibody fragments. Q J Nucl Med 1998;42:262 – 70.

43. Robinson MK, Doss M, Shaller C, et al. Quantitative immuno-positron emission tomography imaging of HER2-positive tumor xenografts with an iodine-124 labeled anti-HER2 diabody. Cancer Res 2005;65:1471 – 8.

44. Al-Lazikani B, Lesk AM, Chothia C. Standard conformations for the canonical structures of immunoglobulins. J Mol Biol 1997;273:927 – 48.